Luminal short chain fatty acids and 5-HT acutely activate myenteric neurons in the mouse proximal colon

C. Fung, B. Cools, S. Malagola, T. Martens, J. Tack, Y. Kazwiny, P. Vanden Berghe*

Laboratory for Enteric NeuroScience (LENS)

Translational Research Center for Gastrointestinal Disorders (TARGID), University of Leuven, Leuven, Belgium

***Correspondence:** Pieter Vanden Berghe, pieter.vandenberghe@kuleuven.be

Pieter Vanden Berghe https://orcid.org/0000-0002-0009-2094

Candice Fung https://orcid.org/0000-0002-4277-3664

Running title: Microbial metabolites activate enteric nerves

ABSTRACT

Background: Gastrointestinal (GI) function is critically dependent on the control of the Enteric Nervous System (ENS), which is situated within the gut wall and organized into two ganglionated nerve plexuses: the submucosal and myenteric plexus. The ENS is optimally positioned and together with the intestinal epithelium, is well-equipped to monitor the luminal contents such as microbial metabolites, and to coordinate appropriate responses accordingly. Despite the heightened interest in the gut microbiota and its influence on intestinal physiology and pathophysiology, how they interact with the host ENS remain unclear. **Methods:** Using full thickness proximal colon preparations from transgenic Villin-CreERT2;R26R-GCaMP3 and Wnt1-Cre;R26R-GCaMP3 mice, which express a fluorescent Ca^{2+} indicator in their intestinal epithelium or in their ENS respectively, we examined the effects of key luminal microbial metabolites (SCFAs and 5-HT) on the mucosa and underlying enteric neurons. **Key Results:** We show that the SCFAs acetate, propionate, and butyrate, as well as 5-HT can, to varying extents, acutely elicit epithelial and neuronal Ca^{2+} responses. Furthermore, SCFAs exert differential effects on submucosal and myenteric neurons. Additionally, we found that submucosal ganglia are predominantly aligned along the striations of the transverse mucosal folds in the proximal colon. **Conclusions & Inferences:** Taken together, our study demonstrates that different microbial metabolites, including SCFAs and 5-HT, can acutely stimulate Ca^{2+} signaling in the mucosal epithelium and in enteric neurons.

Keywords: Colon, Enteric Nervous System, Enteric neurons, Serotonin, Microbiota

INTRODUCTION

The role of the microbes in gut homeostasis and its interaction with the nervous system has gained immense attention in recent years, owing to its implications on health and in a diverse range of disease states such as neurodegeneration and autism spectrum disorders (Cryan et al., 2019; Israelyan and Margolis, 2019; Obata and Pachnis, 2016). The initial point of contact between the microbiota and the host is the intestinal epithelium, which is in turn densely innervated by sensory neurons and secretomotor neurons from the underlying enteric nervous system (ENS). This is an extensive neural network organized in two ganglionated plexuses - the submucosal and myenteric plexus. The submucosal plexus is mainly responsible for regulating fluid secretion, while the myenteric plexus is critical for the control of intestinal motility. Contained within these plexuses are sensory, inter- and motor neurons that innervate and interact with a myriad of different cell types within the gut wall to coordinate integrated gastrointestinal function (Fung and Vanden Berghe, 2020; Furness, 2012; Schneider et al., 2019). Thus, the ENS is in an optimal position to detect and respond to microbial factors in the luminal environment, and a means by which microbiota may influence intestinal physiology (Aktar et al., 2020; Obata et al., 2020). Nonetheless, the mechanisms underlying communication between microbes and their metabolites in the gut lumen, and the host ENS are only beginning to be unraveled.

How the enteric circuitry is modulated by microbes is not well established, but there is good evidence that the intestinal microbial composition affects the properties of enteric neurons. Electrophysiology studies have demonstrated that the electrical excitability of myenteric AH neurons is reduced in germ-free (GF) mice compared to conventionalized germ-free mice and specific pathogen-free (SPF) controls (McVey Neufeld et al., 2013; McVey Neufeld et al., 2015).

Recent work also unveiled a novel molecular mechanism where the gut microbiota was shown to influence the transcription profile of enteric neurons and via the activation of acryl hydrocarbon receptor (AhR) signaling, can ultimately influence colonic motility (Obata et al., 2020). Furthermore, another recent study has shown that a dominant gut commensal in humans, *Bacteroides thetaiotaomicron* (Bt), affects the neurochemical characteristics of the ENS and its innervation of the mucosal epithelium using GF, SPF, and Bt mono-colonized GF mice (Aktar et al., 2020).

The question remains how microbial signals may be detected by the ENS given that the intestinal epithelial barrier separates it from the luminal contents. It has been proposed that crosstalk between the microbiota and ENS may be mediated through microbiota-derived neurotransmitters i.e. serotonin (5-HT), dopamine, acetylcholine (ACh) and gamma aminobutyric acid (GABA) (Margolis et al., 2016). However, the luminal concentrations of these transmitters and whether they actually reach the ENS to modulate neuronal activity are unclear. Another possibility is that intrinsic sensory nerves acutely detect mucosal microbial products through the chemosensing of bacterial metabolites via specialized enteroendocrine cells (EECs) in the epithelium, which are well-equipped with an extensive range of nutrient-sensing receptors and transporters (Blackshaw et al., 2007; Depoortere, 2014). As lipophilic substances may also cross the epithelium by passive diffusion, this is another route by which microbial factors may gain access to the ENS. Notably, short chain fatty acids (SCFAs) are key candidates for mediating the interactions between microbiota and the ENS. Amongst the most prominent products of microbial fermentation in the large bowel are the SCFAs acetate, propionate and butyrate, which are present at concentrations of up to 100 mM in the lumen of the proximal colon (Cummings et al., 1987; Smith et al., 2013). Interestingly, different SCFAs

have been shown to differentially modulate motility patterns in guinea pig colonic segments *in vitro* (Hurst et al., 2014). EECs express several receptors that enable it to detect SCFAs, such as free fatty acid receptor 2 (FFAR2 or GPR43) and 3 (FFAR3 or GPR41). FFAR2 couples to $G\alpha_{q/11}$ and $G\alpha_{i/o}$, and hence signals via both intracellular Ca^{2+} and cyclic adenosine monophosphate (cAMP) secondary messenger systems. On the other hand, FFAR3 couples exclusively to $G\alpha_{i/o}$ and is primarily associated with reducing cAMP levels (Priyadarshini et al., 2018). Some enteric neurons express FFAR3 (Kaji et al., 2016; Nøhr et al., 2013). However, it is unclear whether SCFAs signal indirectly to neurons via EECs, or if they cross the epithelium to act directly on enteric neurons. Moreover, it has not been examined whether the ENS is capable of differentiating between specific luminal SCFAs to potentially trigger differential physiological responses.

Gut microbes may also influence ENS activity through the modulation of serotonergic signaling via SCFAs, which has been shown to increase both the density of 5-HT producing enterochromaffin (EC) cells and their expression of the 5-HT synthesizing enzyme *TPH1* (Reigstad et al., 2015; Yano et al., 2015). 5-HT is one of the most well-studied signaling mediators in mucosal sensory transduction. 5-HT is released from EC cells upon activation by chemical or mechanical stimuli and can act on 5-HT3 receptor expressing intrinsic sensory nerve endings that supply the mucosa (Bellono et al., 2017; Bertrand et al., 1997; Bertrand et al., 2000; Hao et al., 2020). Recent findings further suggest that 5-HT levels in the lumen, which is influenced by the microbiota (Hata et al., 2017), can reciprocally affect microbiota composition and the severity of DSS-induced colitis (Kwon et al., 2019). While these findings collectively implicate luminal SCFAs and the basolateral release of 5-HT in regulating ENS and

gut function through long term interactions, the acute effect of luminal 5-HT on the ENS remains unclear.

The mouse proximal colon contains transverse mucosal folds or ridges and notably houses specific microbial populations underneath the folds that are distinct from those in the luminal digesta (Nava et al., 2011). Moreover, these mucosal folds are thought to play a structural role in slowing the flow of luminal contents and in microbial retention by trapping bacteria-containing components of the digesta (Holtenius and Björnhag, 1985; Hugenholtz and de Vos, 2018; Kamphuis et al., 2017). This raises interesting questions as to whether there are regional specializations in the detection of microbial content at the surface of the mucosal ridges compared to flatter surfaces between the ridges, and whether there are potential differences in the innervation of these regions. The specific organization of the ENS in relation to these mucosal striations has not been examined.

Using full thickness preparations of proximal colon from transgenic Villin-CreERT2;R26R-GCaMP3 (Villin|GCaMP3) and Wnt1-Cre;R26R-GCaMP3 (Wnt1|GCaMP3) mice, which express the fluorescent Ca^{2+} indicator in their intestinal epithelium or in their enteric neurons and glia respectively, we investigated how key microbial metabolites including SCFAs and 5-HT in the gut lumen may signal from the mucosa to the underlying enteric neurons. We also examined the ultrastructure of mucosa and ENS in the proximal colon using fluorescence and second harmonic generation (SHG) microscopy. Our findings show that SCFAs and 5-HT can, to varying extents, elicit epithelial and neuronal Ca^{2+} responses. Further, SCFAs were observed to exert differential effects on myenteric and submucosal neurons. Notably, we also found that the

patterning of submucosal ganglia is arranged such that they closely align with the striations of the transverse mucosal folds in the proximal colon.

METHODS AND MATERIALS

Animals

Adult male and female Wnt1-Cre;R26R-GCaMP3 (Wnt1|GCaMP3) and Villin-CreERT2;R26R-GCaMP3 (Villin|GCaMP3) mice from a C57BL/6 background, receiving a normal diet (Sniff; Soest) and water *ad libitum*, were used in this study (Zariwala et al., 2012). No sex differences in epithelial and neuronal responses to luminal SCFAs or 5-HT were observed within our datasets. Thus, pooled data from male and female mice are presented. Wnt1|GCaMP3 mice express the fluorescent Ca^{2+} indicator GCaMP3 in all enteric neurons and enteric glial cells, while the Villin|GCaMP3 mice express GCaMP3 in the gut epithelium (Boesmans et al., 2018; el Marjou et al., 2004). The mice were killed by cervical dislocation and the intestines were immediately dissected and collected in Krebs solution (120.9 mM NaCl, 5.9 mM KCl, 1.2 mM $MgCl_2$, 1.2 mM NaH_2PO_4, 11.5 mM glucose, 14.4 mM $NaHCO_3$, 2.5 mM $CaCl_2$) bubbled with 95% O_2|5% CO_2. All procedures are approved by the Animal Ethics Committee of the University of Leuven.

Tissue preparation

Tissues were dissected under a stereomicroscope. For both Villin|GCaMP3 and Wnt1|GCaMP3 tissues, the proximal colon was opened along the mesenteric border, and stretched and pinned flat with the mucosa facing up on a silicone elastomer-coated dish filled

with carbogenated Krebs. Luminal contents were carefully removed, ensuring not to damage the mucosa. For Wnt1|GCaMP3 tissues, the tissue was stabilized by stretching it over an inox ring and clamping it in place with a rubber O-ring to minimize contractions (Li et al., 2019; Vanden Berghe et al., 2002). Up to two preparations were obtained from each colon segment. At least N = 3 mice were examined for each set of experiments, unless otherwise specified.

Ca^{2+} imaging of the intestinal epithelium using Villin|GCaMP3 tissue

Villin|GCaMP3 tissue preparations were imaged at room temperature (RT) using a Leica M165 FC fluorescent stereomicroscope (Leica), fitted with an X-Cite 200DC Stabilized Fluorescence Light Source (Lumen Dynamics) and an ORCA-Flash4.0 V3 Digital CMOS camera (Hamamatsu). The mucosa was perfused with stimulating solutions using a micropipette tip positioned at the edge of the imaged field of view. Perfusion was achieved through a gravity-assisted tubing system. Preparations were continuously superfused with Krebs solution bubbled with 95% O_2|5% CO_2 throughout the experiment. Images were recorded at 2 Hz for a duration of 2 min, with 5 min between each recording.

Spinning disk confocal and widefield Ca^{2+} imaging of the ENS using Wnt1|GCaMP3 tissue

Live Ca^{2+} imaging of Wnt1|GCaMP3 ring preparations was performed on two microscopy setups. A set of experiments were conducted at RT using an inverted spinning disk confocal microscope (Nikon Ti – Andor Revolution – Yokogawa CSU-X1 Spinning Disk [Andor, Belfast, UK]) equipped with a Nikon 20× lens (NA 0.8). GCaMP3 was excited at 488 nm and 3-dimensional (3D) stacks were acquired (50 µm) every 2 s over a duration of 4 min using a Piezo

Z Stage controller. For widefield imaging, ring preparations were imaged using a 20x objective lens on a Nikon Eclipse TE300 inverted microscope (Nikon), fitted with a Polychrome V monochromator (TILL Photonics) and Sensicam-QE (PCO Imaging). GCaMP3 was excited at 470 nm and images were recorded for 2 min at 2 Hz using TILLVision software (TILL Photonics). Preparations were continuously superfused with Krebs solution bubbled with 95% O_2|5% CO_2. Stimulating solutions were superfused on to the mucosa via a gravity assisted tubing system (±1 ml/min) using a micropipette tip positioned above the imaged field of view. Stimuli were applied for 1 min and each preparation was exposed to a maximum of 3 different stimuli, with at least a 5 min washout period of Krebs perfusion between stimuli. Experiments were limited to within 3 h following tissue collection to minimize compromised mucosal integrity.

Nutrients and drugs

The microbiota in the hindgut produces high concentrations of SCFAs and total concentrations of SCFA in the mammalian colon are approximately 100 mM (Rechkemmer et al., 1988) with acetate, propionate and butyrate comprising ~ 95% of total SCFAs (Canfora et al., 2015). Concentrations of acetate, propionate, and butyrate in mouse fecal pellets and are in the order of ~37mM, 4mM, and 4mM respectively (Segers et al., 2019). However, 95% of the produced SCFAs are rapidly absorbed by the colonocytes in the caecum and large bowel while only the remaining 5% is secreted in the feces (den Besten et al., 2013). Therefore, the proximal colon is likely to be exposed to much higher concentrations than that detected in the feces. We tested for differences between individual SCFAs at 100 mM each, to circumvent potential confounding effects due to differences in their concentrations. Acetate (100 mM) was prepared with acetic acid (100 mM; Emsure) in a modified Krebs solution (in which the

concentration of NaCl was reduced to 20 mM to correct for osmolarity) and neutralized using NaOH (1 M). Sodium butyrate (100 mM), and sodium propionate (100 mM) (both from Sigma) were also prepared in a modified Krebs solution with reduced NaCl concentration to correct for osmolarity. A SCFA mixture (100µM and 100 mM) containing acetate, propionate and butyrate in a 3:1:1 molar ratio was also tested. The pH of the nutrient solutions was adjusted to 7.4.

Electrochemical measurements of mucosal 5-HT release using a carbon fibre electrode positioned close to the mucosal surface or compressing the mucosa show that concentrations range from ~2 µM at steady state up to ~15 µM with compression-evoked release in *ex vivo* preparations of mouse distal colon (Bertrand and Bertrand, 2010). Measurements of luminal 5-HT in mouse colon by HPLC also show that levels can reach up to approximately 8 µM (Hata et al., 2017). Based on these studies, we applied 5-HT (10 µM) to the mucosal surface in our experiments to mimic luminal 5-HT levels. 5-HT (Sigma) was prepared as a stock solution stored at -20°C and diluted to the final concentration using standard Krebs solution on the day of the experiment.

Data analysis

Recordings of Villin|GCaMP3 tissues were aligned using the linear stack alignment with SIFT plugin for Fiji (Rueden et al., 2017; Schindelin et al., 2012). Analysis of recordings was performed using custom-written routines in Igor Pro 6 (WaveMetrics). For each Villin|GCaMP3 recording, regions of interest were drawn around three different crypts and their Ca^{2+} signal intensity over time was calculated. For Wnt1|GCaMP3 recordings, regions of

interest were drawn within the cytoplasm of active neurons, since GCaMP3 is not expressed in the nucleus of neurons. Values were normalized to the baseline fluorescence intensity and the maximum change in fluorescence from baseline (ΔFi/F0) was calculated for each region of interest. Responses were considered when the Ca^{2+} signal increased above baseline by at least 5 times the intrinsic noise. Fluorescence intensity changes over time in image stacks were analyzed by splitting them into sub-stacks containing the submucosal plexus and myenteric plexus. Statistical analysis was performed using the GraphPad Prism 6 software. For multiple comparisons, a one-way ANOVA with a Bonferroni *post hoc* test was used to test for differences between groups. To test for difference between two groups, an unpaired two-tailed t-test was used. $P < 0.05$ was considered statistically significant. The data visualization tool Plotly was used to generate a 3D plot representing the amplitudes of Ca^{2+} transients (ΔFi/F0) for each active neuron, colour-coded for the SCFA or set of SCFAs it responded to (Inc, 2015).

***Post hoc* immunohistochemistry**

After imaging, some Wnt1|GCaMP3 tissues were fixed using 4% formaldehyde/PBS (Sigma-Aldrich) for 2 h at RT for *post hoc* immunostaining. After washing in PBS (3 x 10 min), the tissues were stored in fresh PBS at 4°C until further processing.

The mucosa, SMP and the circular muscle layer were removed from the fixed tissues by microdissection. The resulting myenteric plexus-longitudinal muscle (LMMP) preparations were incubated for 2 h at RT in blocking solution (4% donkey serum (Merck Millipore)/0.5% Triton-X 100 (Sigma) in PBS). Next, the samples were incubated at 4°C overnight with the

primary antibodies (Table 2). After washing with PBS (3 x 10 min), the samples were incubated with the secondary antibodies for 2 h at RT (Table 3). Following another set of washes in PBS (3 x 10 min), the samples were mounted using Citifluor mounting medium (Citifluor Ltd.). Images were obtained using an LSM 780 confocal microscope (Zeiss) fitted with an argon laser (488 nm) and two solid state lasers (405 and 561 nm). Confocal micrographs display maximum projections of confocal z-stacks. Images were adjusted for brightness and contrast. Neuronal cell counts were performed in ImageJ/Fiji.

Cryosections of Villin|GCaMP3 tissue

Proximal colon from Villin|GCaMP3 mice was cleaned of residual fat and mesentery, cut open along the mesenteric border and pinned flat on a silicone elastomer-coated dish with the mucosal side up. The tissue was then cleaned of feed residues and fixed at RT in 4 % paraformaldehyde/0.2 M phosphate buffer for 1 h. After washing with phosphate buffered saline (PBS), the fixed tissue was put in a 30% sucrose solution and stored at 4 °C for at least 48 h. The tissue was then embedded in OCT compound (Tissue-Tek) and frozen in liquid N_2. Transverse cryosections (50 µm) were cut and collected onto SuperFrostPlus slides (Thermo Scientific). After washing 5 min with PBS, samples were incubated for 2 h at RT in a blocking solution containing 4% donkey serum/0.5% Triton-X 100 in PBS. Afterwards, the samples were incubated at 4 °C overnight with rabbit anti- neuronal class III β-tubulin (Tuj1; Covance, Cat. No. PRB-435P-100, RRID: AB_291637) at a 1:2000 dilution in blocking solution, before washing in PBS (3 x 10 min). The tissues were incubated with donkey anti-rabbit Alexa Fluor 594 (Molecular Probes) at a 1:1000 dilution in blocking solution, for 2 h at RT. After washing in PBS (3 x 10 min), DAPI (1:5000; Invitrogen) was added to each of the samples and incubated at RT

for 5 min. Thereafter, the samples were mounted on the slide using Citifluor mounting medium (Citifluor Ltd.). Images were acquired using an LSM 780 confocal microscope (Zeiss) as described above and adjusted for brightness and contrast.

2-photon excitation fluorescence (2PEF) and second harmonic generation (SHG) imaging

To examine the structure of the proximal colon, we acquired tile Z-stacks of fixed Wnt1|GCaMP3 wholemount tissue on an LSM 780 confocal microscope (Zeiss) using a water-immersion 25x objective (NA 0.8, Zeiss). A tuneable Mai Tai DeepSee Titanium-Sapphire femtosecond laser (680–1050 nm; Spectra-Physics) was used for 2-photon-excited fluorescence (2PEF) imaging and second harmonic generation (SHG) imaging with an excitation wavelength of 850 nm. 2PEF (emission filter: 500–550 nm) and SH (emission filter: 380–430 nm) images were acquired with BiG (GaAsP) non-descanned detectors (Zeiss) in the forward and backward detection beam paths, respectively. An air condenser (NA 0.8) was used for recording forward SH signals. Tile Z-stacks were recorded with spline interpolated Z brightness correction and reconstructed using online stitching with ZEN software (Zeiss). Maximum projections of the slices in the Z stacks containing the mucosal ridge, and submucosal and myenteric layers were performed in ImageJ/Fiji. The blend render of the cross section of the proximal colon containing a striation (136.5 µm x 1026 µm x 91 µm) was created in Imaris. Images were adjusted for brightness and contrast.

RESULTS

The colonic mucosa displays Ca^{2+} responses to bacterial metabolites

We first aimed to establish whether bacterial metabolites including SCFAs and 5-HT can elicit Ca^{2+} responses in the epithelium. To test this, flat regions of the proximal colon mucosa were imaged while acutely perfusing SCFA or 5-HT solutions onto the epithelial surface in full thickness preparations from Villin|GCaMP3 mice (**Fig. 1**).

Calcium responses to individual SCFAs acetate (100 mM), propionate (100 mM) and butyrate (100 mM), and 5-HT (10 µM) were observed (**Fig. 1D**). Of the three SCFAs, acetate elicited the greatest increase in Ca^{2+} signal intensity ($\Delta Fi/F0 = 0.21 \pm 0.04$; $P < 0.0001$; One-way ANOVA with Bonferroni post test). Propionate and butyrate also showed a significantly increased response when compared to baseline ($\Delta Fi/F0 = 0.19 \pm 0.03$; $P < 0.0001$ and $\Delta Fi/F0 = 0.14 \pm 0.02$; $P < 0.01$ respectively). The mucosal application of 5-HT also elicited Ca^{2+} responses, indicating that luminal 5-HT can indeed exert effects on the epithelium. To determine whether any small change in perfusion pressure would be sufficient as a mechanical stimulus to elicit mucosal Ca^{2+} responses, we switched between different perfusion lines filled with Krebs solution. However, this did not evoke a detectable Ca^{2+} signal, indicating that the responses to stimuli tested were not due to a pressure effect.

Ultrastructure of mucosa and plexus layers in the proximal colon

The colonic mucosa lacks the typical villi that are present in the small intestine, rather the outer surface of the epithelium is relatively flat, while the inner surface comprises inward folds (i.e. crypts) (Rubio and Schmidt, 2018). Moreover, in the proximal colon, the mucosa is not a uniform flat sheet but forms unique ridges, which appear as striations that run diagonally along the length of the gut (Sibaev et al., 2003) (**Fig. 2A**). How the ENS is organized relative to these mucosal striations is unknown. Hence, we explored the innervation as well as the

distribution of submucosal and myenteric enteric ganglia in relationship to these structures. Cross-sections (50 μm) through the mucosal striations of the proximal colon show that they are densely innervated by Tuj1^{+} fibers (**Fig. 2B**). We next examined the organization of ENS at a mucosal fold of a wholemount preparation using 2-photon-excited fluorescence and second harmonic generation (SHG) microscopy to image the GCaMP-expressing ENS and collagen, respectively. Upon closer inspection of the distribution of submucosal ganglia in the proximal colon, we found that the submucosal ganglia were indeed predominantly situated beneath and alongside the mucosal striations (**Fig. 2C-E**). On the other hand, myenteric ganglia were evenly distributed within the plexus.

Submucosal and myenteric neurons respond to luminal microbial metabolites in the proximal colon

Having determined that bacterial metabolites can acutely stimulate mucosal Ca^{2+} responses, we next examined the effects of the mucosal application of a SCFA and of 5-HT (10 μM) on the submucosal and myenteric neurons directly below the application site. From preliminary data, we found that of the SCFAs tested, propionate (100 mM) evoked the most robust myenteric neuronal response. In addition, previous work has shown that luminal propionate elicit effects on colonic anion secretion at least in part via submucosal neurons (Tough et al., 2018). Thus, propionate was used in the following experiments. To examine the submucosal and myenteric responses, we imaged in 3D, full thickness preparations of proximal colon from Wnt1|GCaMP3 mice using spinning disk confocal microscopy (**Fig. 3**). As suggested by the morphological data (**Fig. 2**), the only regions in which we could capture both myenteric and submucosal ganglia within a single volume were predominantly areas in close proximity to the

mucosal ridges. Thus, the submucosal data shown were collected only from regions close to the ridges. To also examine possible local regional differences in responses, we compared recordings of the myenteric plexus in which stimuli were perfused onto the mucosal ridges or in the flatter regions of mucosa between the folds. However, these structural differences did not appear to have an effect on the proportions of propionate and 5-HT myenteric responders as they were comparable between regions. Thus, pooled data from both mucosal regions are presented for myenteric responses. Submucosal responses to the mucosal perfusion of 5-HT was especially variable, with a subset of submucosal neurons (13 ± 9%) displaying Ca^{2+} transients during its application (n = 5 ganglia), while propionate elicited responses in only 4 ± 2% of submucosal neurons within the field of view (n = 4 ganglia) (**Fig. 2**). By contrast, a greater proportion of myenteric neurons displayed Ca^{2+} transients during the perfusion of propionate compared to 5-HT (8 ± 2% vs. 2 ± 1%, respectively, n = 8 ganglia; unpaired t-test, P = 0.03) (**Fig. 3**).

Different SCFAs applied to the mucosa activate different patterns of myenteric neurons

With the mucosal application of a SCFA mixture (100 mM) containing acetate, propionate and butyrate in a 3:1:1 molar ratio, Ca^{2+} transients were observed in a higher proportion of myenteric neurons (11 ± 2%; P < 0.01 vs. baseline) than those displaying spontaneous Ca^{2+} activity at baseline (**Fig. 4A**). It is possible that SCFAs exert effects on the ENS after crossing the epithelium or via the blood stream, albeit at lower concentrations than in the lumen with levels of SCFA in the circulation reaching up to 100 µM (Tough et al., 2018). To test whether neuronal Ca^{2+} responses to the SCFA mixture may involve a direct effect on neurons, we examined responses to two repeated applications of the SCFA mixture (100 µM; 30 s) onto

peeled myenteric plexus preparations separated by a 5 min Krebs washout. However, no consistent responses to the direct application of the SCFA mixture were observed with the number of active neurons during the 1st and 2nd applications (7 ± 1% and 6 ± 1%, respectively; n = 12 ganglia; N = 6 mice examined) being comparable to that observed at baseline (7 ± 1%; n = 5 ganglia; N = 2 mice examined). Since acetate, propionate and butyrate have been reported to differentially modulate colonic motility *in vitro* (Hurst et al., 2014), we next tested whether these selected SCFAs individually applied to the mucosa may activate specific patterns of myenteric neurons. The mucosal application of acetate (100mM), propionate (100mM) and butyrate (100mM), each elicited Ca^{2+} transients in a higher proportion of neurons than that spontaneously active before stimulation (**Fig. 4A**). Propionate activated the greatest number of neurons within the field of view (17 ± 2%; $P < 0.0001$ vs. baseline), while acetate and butyrate both evoked a response in 9 ± 1% of neurons. The change in perfusion pressure from switching between different perfusion lines filled with Krebs solution (N = 2 animals) did not evoke any significant neuronal Ca^{2+} responses above baseline activity (4 ± 1% vs. 6 ± 1% respectively; $P > 0.05$). Propionate was observed to elicit a response in a greater percentage of neurons in these widefield recordings (**Fig. 4A**) compared to the spinning disk confocal recordings (**Fig. 3B**). This may be at least partly attributed to a technical difference in the ease of positioning the perfusion pipette between the two systems.

To then assess whether different SCFAs activated specific patterns of myenteric neurons, we analyzed the neurons that responded to one or more of the SCFA solutions, where the sequence of SCFA application was varied between experiments. Of all the neurons responding to mucosally-applied acetate, 66 ± 7% responded to propionate and 47 ± 7% responded to

butyrate, while 19 ± 4% responded only to acetate (n = 10 ganglia examined). The percentages of propionate responders that also responded to acetate and butyrate, were 43 ± 9% and 38 ± 6% respectively, and 42 ± 9% responded only to propionate. Of neurons responding to butyrate, 46 ± 7% responded to acetate, 65 ± 8% responded to propionate, and 21 ± 5% responded only to butyrate. These data suggest that different SCFAs present in the gut lumen can acutely activate different neuronal populations. Even though there is a substantial overlap in the responsive neurons, also some unique responders were observed for each SCFA (**Table 1**). Despite these specific responder proportions, there were no apparent differences in the amplitudes or their distribution between neurons that responded to only one, a combination, or all three of the SCFAs tested (**Fig. 4B**). Additionally, we compared the neurochemical coding of responding neurons to determine whether specific neuronal subtypes were responsive to different SCFAs using *post hoc* labelling for markers of two major subsets of myenteric neurons, that is, nNOS and calretinin. nNOS-immunoreactive neurons are typically inhibitory motor or interneurons, while calretinin-immunoreactive neurons include excitatory motor and interneurons (Sang and Young, 1998). However, there were no significant differences in the relative proportions of neuronal nitric oxide synthase (nNOS)- and calretinin-immunoreactive neurons that responded to each of the SCFAs overall (n = 4 ganglia; **Fig. 5**). While we also examined the neurochemistry of neurons that responded uniquely to only one of SCFAs (**Table 1**), the numbers of neurons identified were too low to draw substantial conclusions.

DISCUSSION

The functional output of enteric circuitry is an important means through which gut microbes can influence gut function. In this study, we examined how key microbial metabolites in the lumen, namely SCFAs and 5-HT, may acutely signal from the epithelium to the underlying enteric network of submucosal and myenteric neurons. We found that while SCFAs and 5-HT applied to the epithelial surface elicit similar amplitude Ca^{2+} responses, SCFAs were more effective in evoking myenteric neuronal Ca^{2+} responses than 5-HT. By contrast, in the submucosal plexus, Ca^{2+} transients observed in submucosal neurons during the mucosal application of 5-HT and propionate were largely variable between preparations. We further demonstrate that different SCFAs activate different patterns of myenteric neurons, albeit with a substantial overlap in the neuronal responders. Interestingly, we also found that the submucosal ganglia are organized such that they are predominantly aligned along the mucosal striations in the proximal colon.

Our results point to possible localized variations in the enteric innervation of the mucosal epithelium. In particular, the specific arrangement of submucosal ganglia might be indicative of a specialized submucosal innervation of the mucosal ridges. The striations of the proximal colon have been proposed to have a structural role in slowing the flow of luminal contents, acting to trap the bacteria-containing components of the digesta between the mucosal striations such that microbial content can subsequently be transported back to the caecum via anti-peristaltic contractions (Holtenius and Björnhag, 1985; Hugenholtz and de Vos, 2018; Kamphuis et al., 2017). Early studies in which labelled bacteria were infused into the proximal colon of guinea pigs showed that the concentration of the marker found between the mucosal striations was double that detected in the luminal contents, and that the marker could also be

traced to the caecal contents (Holtenius and Björnhag, 1985). Thus, the mucosal structures may serve as a means of microbial retention. Whether the specific organization of submucosal plexus in this region, where ganglia are predominantly clustered beneath and along the mucosal ridges, may contribute to this process is yet to be determined. It may be that secretomotor neurons preferentially innervate these structures to regulate mucus and fluid secretions to facilitate the trapping of bacterial content and its transport. On the other hand, the development of this SMP organization might be influenced by microbial colonization during early postnatal ages. Indeed, submucosal ganglia in the colon begin to form shortly after birth and continue to mature postnatally (between postnatal days 3 – 28) (McKeown et al., 2001), and this coincides with the developmental time window during which much of the early gut microbiota is established (Foong et al., 2020). An intriguing possibility is that submucosal ganglia may preferentially form close to and innervate the mucosal folds where microbes accumulate and reside. Further studies are necessary to determine whether there are in fact differences in the specific innervation of the mucosal ridges by submucosal neurons and to explore the influence of microbiota on SMP development in the proximal colon during early postnatal ages. Unlike in the submucosa, myenteric ganglia were observed to be relatively evenly distributed within the plexus. Further, no apparent differences in the myenteric responses to propionate and 5-HT were observed when stimuli were applied onto the mucosal ridges compared to when applied between the ridges.

We also found that the application of 5-HT to luminal surface of the colonic mucosa was not an effective stimulus in stimulating Ca^{2+} responses in myenteric neurons, with only a small proportion of responding neurons within the field of view despite eliciting clear responses in

the epithelium. Submucosal responses to 5-HT were also largely variable. The role of the 5-HT and 5-HT3 receptor signaling pathway has been extensively examined in the context of mucosal chemosensory transduction and as a link between the external luminal environment and the underlying ENS (Bellono et al., 2017; Bertrand et al., 1997; Bertrand et al., 2000; Hao et al., 2020). Previous studies in small intestine have shown that 5-HT applied to the mucosal surface elicits responses in myenteric intrinsic sensory neurons of exposed regions where the mucosa has been dissected away (Bertrand et al., 2000; Gwynne and Bornstein, 2007). This was recently revisited by taking a more integrated approach using full thickness preparations, where 5-HT was injected into villi of small intestine preparations to better mimic its basolateral release, or applied onto the epithelium, and neuronal responses in the myenteric plexus were imaged (Fung et al., 2021; Hao et al., 2020). Notably, it was reported that 5-HT applied to the epithelial surface evoked detectable myenteric neuronal responses in only 30% of preparations and responses were of a smaller amplitude compared to its application into villi (i.e. directly onto mucosal nerve endings) (Hao et al., 2020). These results taken together with our findings may allude to different roles of 5-HT that is released into the lumen as compared to its basolateral release and involvement in sensory transduction. Recent work has shown that luminal 5-HT acts to decrease the virulence of pathogenic enteric bacteria that express CpxA, a bacterial membrane-bound serotonin receptor (Kumar et al., 2020). Thus, while basolaterally-released 5-HT from EC cells may act as a sensory mediator and acutely activate enteric neurons, levels of 5-HT secreted into the lumen may be monitored by the ENS via a different mechanism, likely involving a broader activation of the mucosal epithelium.

The effects of SCFAs on various aspects of colonic motility, secretion, and enteric neurons have been reported in a number of studies (Hurst et al., 2014; Kaji et al., 2016; Mitsui et al., 2005; Ono et al., 2004; Soret et al., 2010). However, to our knowledge, this is the first detailed examination of how luminal SCFAs influence enteric neuronal activity in colonic preparations with the layers of gut wall intact. We found that acetate, propionate, and butyrate each evoked Ca^{2+} responses in the mucosal epithelium with comparable amplitudes but there were subtle differences in the pattern of myenteric neurons activated. Of the three SCFAs tested, propionate was shown to elicit the greatest response with approximately 18% of myenteric neurons responding within the field of view. Whether SCFAs may stimulate enteric neurons directly or indirectly remains to be addressed. In addition to the activation of EECs, SCFAs can also be transported into epithelial cells (Iwanaga and Kishimoto, 2015). Butyrate in particular is mainly metabolized within the cell and provides a major energy source for colonocytes, while propionate and acetate can traverse the epithelium and enter the circulation (Cummings et al., 1987). Hence, it is possible that luminal SCFAs may not only be detected by enteric neurons via EECs but might also signal directly to enteric nerve endings in the mucosa. Indeed, FFAR3 has been shown to be expressed in nerve endings that wrap around the base of the crypts in the rat proximal colon, although whether these are of intrinsic or extrinsic origin is unknown (Kaji et al., 2016). We demonstrated that the direct application of a SCFA mixture to peeled myenteric plexus preparations with the mucosa removed did not elicit consistent neuronal Ca^{2+} responses, indicating that responses observed in full thickness preparations is not due to a direct effect of SCFAs on neuronal cell bodies. These findings also indicate that the mucosa is necessary to transduce the luminal SCFA signals. Propionate and butyrate, but not acetate, have been previously shown to stimulate contractile activity in circular muscle strips of rat distal colon and notably, propionate-evoked responses were not observed in

preparations lacking mucosa (Mitsui et al., 2005). Subsequent pharmacological analysis showed that a component of the propionate-induced response was neurally mediated, involving the activation of 5-HT4 receptors and cholinergic motor neurons (Mitsui et al., 2005). While these findings implicate the involvement of 5-HT release from EC cells, which express the SCFA receptors FFAR2 and FFAR3 (Martin et al., 2017a), SCFAs do not acutely stimulate 5-HT release in primary EC cells (Martin et al., 2017b). Whether this holds true for EC cells in their native environment is yet to be established. When we applied SCFAs to the mucosal surface, it was apparent that a large population of epithelial cells showed Ca^{2+} responses. It is likely that not only EC cells but other EECs are involved in transducing the SCFA signal. Further studies are necessary to elucidate whether SCFAs interact with enteric neurons responses via EECs, by directly acting on nerve endings in the mucosa, or a combination of the two.

Upon further assessment of the patterns of myenteric neuronal activation, we found that responders unique to only one of the SCFAs were observed despite a substantial overlap in responders to each SCFA. We compared the neurochemical identity of responding neurons for each SCFA using markers for two major subclasses of myenteric neurons (i.e. nNOS and calretinin) (Sang and Young, 1996; Sang and Young, 1998) and found overall proportion of nitrergic and calretinin^{+} responders did not differ between stimuli and the majority of responders labelled for nNOS. It has been previously reported that different SCFAs differentially modulate motility patterns in guinea pig colonic preparations (Hurst et al., 2014). Whether the specific patterns of myenteric neuronal activity that we observed may contribute to different motor outputs requires further investigation. In addition, considering FFAR2 and

FFAR3 can also signal through cAMP and independently of Ca^{2+}, our use of Ca^{2+} imaging may not have revealed the full extent of responses to SCFAs.

Collectively, our study demonstrates that different microbial metabolites including the SCFAs acetate, propionate, and butyrate, as well as 5-HT can stimulate Ca^{2+} signaling in the mucosal epithelium and to varying extents, in submucosal and myenteric neurons. Future studies will be necessary to further delve into the mechanisms by which these luminal microbial signals are communicated to enteric neurons.

Acknowledgements

The authors acknowledge support from Methusalem (METH/014/05, KU Leuven) and FWO (Fonds voor wetenschappelijk onderzoek) G.093818N and the Erasmus+ programme (University of Rome – KUL). Images were recorded on microscopy equipment in LENS / Cell and tissue Imaging Cluster (CIC), supported by Hercules AKUL/11/37; AKUL/09/50 and FWO G.0929.15.

Data availability statement

The data that support the findings of this study are available from the corresponding author upon reasonable request.

REFERENCES

Aktar, R., Parkar, N., Stentz, R., Baumard, L., Parker, A., Goldson, A., Brion, A., Carding, S., Blackshaw, A. and Peiris, M. (2020). Human resident gut microbe Bacteroides thetaiotaomicron regulates colonic neuronal innervation and neurogenic function. *Gut Microbes*, 1-13.

Bellono, N. W., Bayrer, J. R., Leitch, D. B., Castro, J., Zhang, C., O'Donnell, T. A., Brierley, S. M., Ingraham, H. A. and Julius, D. (2017). Enterochromaffin Cells Are Gut Chemosensors that Couple to Sensory Neural Pathways. *Cell* **170**, 185-198.e116.

Bertrand, P. P. and Bertrand, R. L. (2010). Serotonin release and uptake in the gastrointestinal tract. *Autonomic Neuroscience: Basic and Clinical* **153**, 47-57.

Bertrand, P. P., Kunze, W. A., Bornstein, J. C., Furness, J. B. and Smith, M. L. (1997). Analysis of the responses of myenteric neurons in the small intestine to chemical stimulation of the mucosa. *American Journal of Physiology* **273**, G422-435.

Bertrand, P. P., Kunze, W. A., Furness, J. B. and Bornstein, J. C. (2000). The terminals of myenteric intrinsic primary afferent neurons of the guinea-pig ileum are excited by 5-hydroxytryptamine acting at 5-hydroxytryptamine-3 receptors. *Neuroscience* **101**, 459-469.

Blackshaw, L. A., Brookes, S. J., Grundy, D. and Schemann, M. (2007). Sensory transmission in the gastrointestinal tract. *Neurogastroenterology and Motility* **19**, 1-19.

Boesmans, W., Hao, M. M. and Vanden Berghe, P. (2018). Optogenetic and chemogenetic techniques for neurogastroenterology. *Nature Reviews. Gastroenterology & Hepatology* **15**, 21-38.

Canfora, E. E., Jocken, J. W. and Blaak, E. E. (2015). Short-chain fatty acids in control of body weight and insulin sensitivity. *Nature Reviews Endocrinology* **11**, 577-591.

Cryan, J. F., O'Riordan, K. J., Cowan, C. S. M., Sandhu, K. V., Bastiaanssen, T. F. S., Boehme, M., Codagnone, M. G., Cussotto, S., Fulling, C., Golubeva, A. V., et al. (2019). The Microbiota-Gut-Brain Axis. *Physiol Rev* **99**, 1877-2013.

Cummings, J. H., Pomare, E. W., Branch, W. J., Naylor, C. P. and Macfarlane, G. T. (1987). Short chain fatty acids in human large intestine, portal, hepatic and venous blood. *Gut* **28**, 1221-1227.

den Besten, G., van Eunen, K., Groen, A. K., Venema, K., Reijngoud, D.-J. and Bakker, B. M. (2013). The role of short-chain fatty acids in the interplay between diet, gut microbiota, and host energy metabolism. *J Lipid Res* **54**, 2325-2340.

Depoortere, I. (2014). Taste receptors of the gut: emerging roles in health and disease. *Gut* **63**, 179-190.

el Marjou, F., Janssen, K. P., Chang, B. H., Li, M., Hindie, V., Chan, L., Louvard, D., Chambon, P., Metzger, D. and Robine, S. (2004). Tissue-specific and inducible Cre-mediated recombination in the gut epithelium. *Genesis (New York, N.Y. : 2000)* **39**, 186-193.

Foong, J. P. P., Hung, L. Y., Poon, S., Savidge, T. C. and Bornstein, J. C. (2020). Early life interaction between the microbiota and the enteric nervous system. *American Journal of Physiology-Gastrointestinal and Liver Physiology* **319**, G541-G548.

Fung, C., Hao, M. M., Obata, Y., Tack, J., Pachnis, V., Boesmans, W. and Vanden Berghe, P. (2021). Luminal nutrients activate distinct patterns in submucosal and myenteric neurons in the mouse small intestine. bioRxiv, 2021.2001.2019.427232.

Fung, C. and Vanden Berghe, P. (2020). Functional circuits and signal processing in the enteric nervous system.

Furness, J. B. (2012). The enteric nervous system and neurogastroenterology. *Nature Reviews. Gastroenterology & Hepatology* **9**, 286-294.

Gwynne, R. M. and Bornstein, J. C. (2007). Local inhibitory reflexes excited by mucosal application of nutrient amino acids in guinea pig jejunum. *American Journal of Physiology. Gastrointestinal and Liver Physiology* **292**, G1660-1670.

Hao, M. M., Fung, C., Boesmans, W., Lowette, K., Tack, J. and Vanden Berghe, P. (2020). Development of the intrinsic innervation of the small bowel mucosa and villi. *American Journal of Physiology-Gastrointestinal and Liver Physiology* **318**, G53-G65.

Hata, T., Asano, Y., Yoshihara, K., Kimura-Todani, T., Miyata, N., Zhang, X.-T., Takakura, S., Aiba, Y., Koga, Y. and Sudo, N. (2017). Regulation of gut luminal serotonin by commensal microbiota in mice. *PLoS ONE* **12**, e0180745.

Holtenius, K. and Björnhag, G. (1985). The colonic separation mechanism in the guinea-pig (Cavia porcellus) and the chinchilla (Chinchilla laniger). *Comparative biochemistry and physiology. A, Comparative physiology* **82**, 537-542.

Hugenholtz, F. and de Vos, W. M. (2018). Mouse models for human intestinal microbiota research: a critical evaluation. *Cellular and Molecular Life Sciences* **75**, 149-160.

Hurst, N. R., Kendig, D. M., Murthy, K. S. and Grider, J. R. (2014). The short chain fatty acids, butyrate and propionate, have differential effects on the motility of the guinea pig colon. *Neurogastroenterology and motility : the official journal of the European Gastrointestinal Motility Society* **26**, 1586-1596.

Inc, P. T. (2015). Collaborative data science. *Montréal, QC*.

Israelyan, N. and Margolis, K. G. (2019). Reprint of: Serotonin as a link between the gut-brain-microbiome axis in autism spectrum disorders. *Pharmacological Research* **140**, 115-120.

Iwanaga, T. and Kishimoto, A. (2015). Cellular distributions of monocarboxylate transporters: a review. *Biomedical research (Tokyo, Japan)* **36**, 279-301.

Kaji, I., Akiba, Y., Konno, K., Watanabe, M., Kimura, S., Iwanaga, T., Kuri, A., Iwamoto, K.-i., Kuwahara, A. and Kaunitz, J. D. (2016). Neural FFA3 activation inversely regulates anion secretion evoked by nicotinic ACh receptor activation in rat proximal colon. *Journal of Physiology* **594**, 3339-3352.

Kamphuis, J. B. J., Mercier-Bonin, M., Eutamène, H. and Theodorou, V. (2017). Mucus organisation is shaped by colonic content; a new view. *Scientific Reports* **7**, 8527.

Kumar, A., Russell, R. M., Pifer, R., Menezes-Garcia, Z., Cuesta, S., Narayanan, S., MacMillan, J. B. and Sperandio, V. (2020). The Serotonin Neurotransmitter Modulates Virulence of Enteric Pathogens. *Cell Host & Microbe*.

Kwon, Y. H., Wang, H., Denou, E., Ghia, J.-E., Rossi, L., Fontes, M. E., Bernier, S. P., Shajib, M. S., Banskota, S., Collins, S. M., et al. (2019). Modulation of Gut Microbiota Composition by Serotonin Signaling Influences Intestinal Immune Response and Susceptibility to Colitis. *Cellular and Molecular Gastroenterology and Hepatology* **7**, 709-728.

Li, Z., Hao, M. M., Van den Haute, C., Baekelandt, V., Boesmans, W. and Vanden Berghe, P. (2019). Regional complexity in enteric neuron wiring reflects diversity of motility patterns in the mouse large intestine. *eLife* **8**, e42914.

Margolis, K. G., Gershon, M. D. and Bogunovic, M. (2016). Cellular Organization of Neuroimmune Interactions in the Gastrointestinal Tract. *Trends in immunology* **37**, 487-501.

Martin, A. M., Lumsden, A. L., Young, R. L., Jessup, C. F., Spencer, N. J. and Keating, D. J. (2017a). The nutrient-sensing repertoires of mouse enterochromaffin cells differ between duodenum and colon. **29**.

Martin, A. M., Lumsden, A. L., Young, R. L., Jessup, C. F., Spencer, N. J. and Keating, D. J. (2017b). Regional differences in nutrient-induced secretion of gut serotonin. *Physiological Reports* **5**, e13199.

McKeown, S. J., Chow, C. W. and Young, H. M. (2001). Development of the submucous plexus in the large intestine of the mouse. *Cell and Tissue Research* **303**, 301-305.

McVey Neufeld, K. A., Mao, Y. K., Bienenstock, J., Foster, J. A. and Kunze, W. A. (2013). The microbiome is essential for normal gut intrinsic primary afferent neuron excitability in the mouse. *Neurogastroenterology and Motility* **25**, 183-e188.

McVey Neufeld, K. A., Perez-Burgos, A., Mao, Y. K., Bienenstock, J. and Kunze, W. A. (2015). The gut microbiome restores intrinsic and extrinsic nerve function in germ-free mice accompanied by changes in calbindin. *Neurogastroenterology and Motility* **27**, 627-636.

Mitsui, R., Ono, S., Karaki, S. and Kuwahara, A. (2005). Neural and non-neural mediation of propionate-induced contractile responses in the rat distal colon. *Neurogastroenterology & Motility* **17**, 585-594.

Nava, G. M., Friedrichsen, H. J. and Stappenbeck, T. S. (2011). Spatial organization of intestinal microbiota in the mouse ascending colon. *The ISME Journal* **5**, 627-638.

Nøhr, M. K., Pedersen, M. H., Gille, A., Egerod, K. L., Engelstoft, M. S., Husted, A. S., Sichlau, R. M., Grunddal, K. V., Poulsen, S. S., Han, S., et al. (2013). GPR41/FFAR3 and GPR43/FFAR2 as cosensors for short-chain fatty acids in enteroendocrine cells vs FFAR3 in enteric neurons and FFAR2 in enteric leukocytes. *Endocrinology* **154**, 3552-3564.

Obata, Y., Castano, A., Boeing, S., Bon-Frauches, A. C., Fung, C., Fallesen, T., de Aguero, M. G., Yilmaz, B., Lopes, R., Huseynova, A., et al. (2020). Neuronal programming by microbiota regulates intestinal physiology. *Nature* **578**, 284-289.

Obata, Y. and Pachnis, V. (2016). The Effect of Microbiota and the Immune System on the Development and Organization of the Enteric Nervous System. *Gastroenterology* **151**, 836-844.

Ono, S., Karaki, S.-i. and Kuwahara, A. (2004). Short-Chain Fatty Acids Decrease the Frequency of Spontaneous Contractions of Longitudinal Muscle via Enteric Nerves in Rat Distal Colon. *The Japanese Journal of Physiology* **54**, 483-493.

Priyadarshini, M., Kotlo, K. U., Dudeja, P. K. and Layden, B. T. (2018). Role of Short Chain Fatty Acid Receptors in Intestinal Physiology and Pathophysiology. *Comprehensive Physiology* **8**, 1091-1115.

Rechkemmer, G., Rönnau, K. and von Engelhardt, W. (1988). Fermentation of polysaccharides and absorption of short chain fatty acids in the mammalian hindgut. *Comparative biochemistry and physiology. A, Comparative physiology* **90**, 563-568.

Reigstad, C. S., Salmonson, C. E., Rainey, J. F., 3rd, Szurszewski, J. H., Linden, D. R., Sonnenburg, J. L., Farrugia, G. and Kashyap, P. C. (2015). Gut microbes promote colonic serotonin production through an effect of short-chain fatty acids on enterochromaffin cells. *The FASEB Journal* **29**, 1395-1403.

Rubio, C. A. and Schmidt, P. T. (2018). Morphological Classification of Corrupted Colonic Crypts in Ulcerative Colitis. *Anticancer research* **38**, 2253-2259.

Rueden, C. T., Schindelin, J., Hiner, M. C., DeZonia, B. E., Walter, A. E., Arena, E. T. and Eliceiri, K. W. (2017). ImageJ2: ImageJ for the next generation of scientific image data. *BMC Bioinformatics* **18**, 529.

Sang, Q. and Young, H. M. (1996). Chemical coding of neurons in the myenteric plexus and external muscle of the small and large intestine of the mouse. *Cell and Tissue Research* **284**, 39-53.

---- (1998). The identification and chemical coding of cholinergic neurons in the small and large intestine of the mouse. *The Anatomical Record* **251**, 185-199.

Schindelin, J., Arganda-Carreras, I., Frise, E., Kaynig, V., Longair, M., Pietzsch, T., Preibisch, S., Rueden, C., Saalfeld, S., Schmid, B., et al. (2012). Fiji: an open-source platform for biological-image analysis. *Nature methods* **9**, 676-682.

Schneider, S., Wright, C. M. and Heuckeroth, R. O. (2019). Unexpected Roles for the Second Brain: Enteric Nervous System as Master Regulator of Bowel Function. *Annual Review of Physiology* **81**, 235-259.

Segers, A., Desmet, L., Thijs, T., Verbeke, K., Tack, J. and Depoortere, I. (2019). The circadian clock regulates the diurnal levels of microbial short-chain fatty acids and their rhythmic effects on colon contractility in mice. *Acta Physiologica* **225**, e13193.

Sibaev, A., Franck, H., Vanderwinden, J.-M., Allescher, H.-D. and Storr, M. (2003). Structural differences in the enteric neural network in murine colon: impact on electrophysiology. *American Journal of Physiology-Gastrointestinal and Liver Physiology* **285**, G1325-G1334.

Smith, P. M., Howitt, M. R., Panikov, N., Michaud, M., Gallini, C. A., Bohlooly-Y, M., Glickman, J. N. and Garrett, W. S. (2013). The microbial metabolites, short-chain fatty acids, regulate colonic Treg cell homeostasis. *Science (New York, N.Y.)* **341**, 569-573.

Soret, R., Chevalier, J., De Coppet, P., Poupeau, G., Derkinderen, P., Segain, J. P. and Neunlist, M. (2010). Short-Chain Fatty Acids Regulate the Enteric Neurons and Control Gastrointestinal Motility in Rats. *Gastroenterology* **138**, 1772-1782.e1774.

Tough, I. R., Forbes, S. and Cox, H. M. (2018). Signaling of free fatty acid receptors 2 and 3 differs in colonic mucosa following selective agonism or coagonism by luminal propionate. *Neurogastroenterology & Motility* **30**, e13454.

Vanden Berghe, P., Kenyon, J. L. and Smith, T. K. (2002). Mitochondrial Ca2+ uptake regulates the excitability of myenteric neurons. *Journal of Neuroscience* **22**, 6962-6971.

Yano, J. M., Yu, K., Donaldson, G. P., Shastri, G. G., Ann, P., Ma, L., Nagler, C. R., Ismagilov, R. F., Mazmanian, S. K. and Hsiao, E. Y. (2015). Indigenous bacteria from the gut microbiota regulate host serotonin biosynthesis. *Cell* **161**, 264-276.

Zariwala, H. A., Borghuis, B. G., Hoogland, T. M., Madisen, L., Tian, L., De Zeeuw, C. I., Zeng, H., Looger, L. L., Svoboda, K. and Chen, T. W. (2012). A Cre-dependent GCaMP3 reporter mouse for neuronal imaging in vivo. *Journal of Neuroscience* **32**, 3131-3141.

Figure legends

Figure 1. Imaging of Villin|GCaMP3 mouse proximal colon preparations **A.** Confocal image of a cryosection (thickness 50 µm) from a Villin|GCaMP3 mouse proximal colon showing GCaMP3 expression in the colonic epithelium and staining for Tuj1 (red) and DAPI (blue) to label nerve fibers and cell nuclei, respectively **B.** Simplified schematic depicting the imaging setup. A micropipette tip connected to a gravity-assisted tubing system was used to apply different solutions (e.g. Acetate (A) red; Propionate, (P) green; Butyrate, (B) blue) onto the mucosal surface of full thickness proximal colon preparations while imaging from above **C.** Representative widefield images of the mucosal surface of the proximal colon at baseline and during the application of propionate (100 mM). Colour-coded images show changes in fluorescence intensity throughout the recording, with high intensity changes represented by warmer colours **D.** Graph displaying the changes in fluorescence intensity (ΔFi/F0) in response to different microbial metabolites applied to the epithelial surface. The short chain fatty acids (SCFAs) acetate, propionate, and butyrate, as well as 5-HT each evoked a significant Ca^{2+} response above baseline (*** $P < 0.001$, **** $P < 0.0001$; One-way ANOVA with Bonferroni post-hoc test). No detectable responses were observed in response to the application of Krebs as a negative control. Data are shown as mean ± SEM.

Figure 2. Structure of a mucosal fold in the proximal colon **A.** Simplified schematic illustrating the mucosal striations as observed in the proximal colon when the tissue is cut along the mesenteric border and opened up as a flat sheet. **B.** Confocal image of a cryosection (thickness 50 µm) from a Villin|GCaMP3 mouse proximal colon showing GCaMP3 expression in the colonic epithelium and staining for Tuj1 (red) and DAPI (blue) to label nerve fibers and cell nuclei, respectively. Notably, the mucosal ridge structure is densely innervated. **C-C".** Representative images of a mucosal fold and the underlying submucosal plexus (SMP) and myenteric plexus (MP) of a full thickness ring preparation of Wnt1|GCaMP3 mouse proximal colon. The GCaMP-expressing myenteric plexus and submucosal plexus are depicted in magenta and green, respectively. The collagen supporting the mucosal ridge structure is shown in yellow as detected using label-free second harmonic generation (SHG) imaging. The majority of submucosal ganglia are aligned along the mucosal ridge, while myenteric ganglia are relatively evenly distributed. Scale bars: 100 µm. **D.** Merged overview image of a mucosal fold and underlying nerve plexuses, including the region displayed in C-C" (i) and E (ii). **E.** Blend render of the cross section indicated in C and displayed in the YZ-plane. This render illustrates the typical distribution of myenteric (magenta, GCaMP3) and submucosal ganglia (green, GCaMP3) with respect to the colonic ridge (red, SHG). The submucosal ganglia are predominantly clustered underneath and slightly distal to the mucosal folds, whereas the myenteric plexus is distributed homogeneously along the length of the gut. Scale bar: 100 µm.

Figure 3. Submucosal and myenteric neuronal responses to propionate (100 mM) and 5-HT (10 µM) applied to the mucosa **A.** Schematic showing the imaging setup. A micropipette tip

connected to a gravity-assisted tubing system was used to apply different solutions onto the mucosal surface of full thickness proximal colon ring preparations while the underlying submucosal and myenteric neurons were imaged on an inverted microscope. Submucosal neurons were predominantly situated underneath the mucosal ridges **B.** Graph representing the percentage of submucosal and myenteric neurons within the field of view that responded to propionate or 5-HT, and their response amplitudes (ΔFi/F0). In the submucosal plexus, 3 of 4 ganglia examined showed Ca^{2+} responses to propionate, while 3 of 5 ganglia examined responded to 5-HT. In the myenteric plexus, responses to propionate and to 5-HT were observed in 6 of 8 ganglia examined. The average total number of myenteric and submucosal neurons per field of view were 52 ± 3 and 25 ± 5, respectively. A significantly larger proportion myenteric neurons responded to propionate compared to 5-HT (P = 0.03; unpaired t-test; n = 8 ganglia). Data are presented as mean ± SEM. Representative images of (**C**) submucosal and (**D**) myenteric ganglia and their responses to propionate and 5-HT. Scale bars: 20 µm. Arrows indicate responding neurons and their corresponding Ca^{2+} transients are depicted in the traces below as a change in fluorescence over time. Propionate and 5-HT were applied from 120 – 180s, as indicated by the blue shaded bars.

Figure 4. Myenteric neuronal responses to SCFAs **A.** Graph illustrating the percentage of active myenteric neurons at baseline (n = 32 ganglia) and during the perfusion of Krebs (n = 4), a SCFA mixture (100 mM; n = 6), acetate (100 mM; n = 19), propionate (100 mM; n = 14), or butyrate (100 mM; n = 14) onto the mucosal surface from 20 – 80s. A significantly larger proportion of active myenteric neurons were observed in response to the application of the SCFA mixture and each individual SCFA compared to baseline (* P < 0.05, ** P < 0.01, **** P

< 0.0001; one-way ANOVA with a Bonferroni post test). Of the total ganglia examined, 2/31 ganglia were not responsive to any of the stimuli tested. The average total number of myenteric neurons per field of view was 85 ± 3. Data are presented as mean ± SEM **B.** 3D plot representing the amplitudes of Ca^{2+} transients (ΔFi/F0) for each active neuron, colour-coded for the SCFA or set of SCFAs it responded to. Of note, a number of neurons responded only to one of the three SCFAs tested, but many responded to multiple SCFAs (n = 10 ganglia examined) **C-E'.** Representative image of a myenteric ganglion and its responses to acetate (red), propionate (green), and butyrate (cyan), with responding neurons highlighted by the colour overlay. Arrows mark example responding neurons and their corresponding Ca^{2+} transients are depicted in the traces below as a change in fluorescence over time. The Ca^{2+} transients are colour-coded such that the green traces correspond to signals detected in the neuron that responded only to propionate, the purple traces correspond to signals in the neuron that responded to acetate and propionate, while the yellow traces correspond to signals in the neuron that responded to acetate, propionate, and butyrate. Scale bars: 20 µm.

Figure 5. *Post hoc* immunohistochemical labelling of the myenteric plexus reveals which subtypes of neurons respond to different SCFAs **A-A".** Representative confocal images of a GCaMP3-expressing (green) ganglion stained for neuronal nitric oxide synthase (nNOS, cyan) and calretinin (red) following Ca^{2+} imaging. **B.** Corresponding widefield image of the same ganglion captured during live Ca^{2+} imaging. Arrows indicate responders to acetate (red), propionate (green), and butyrate (blue). **C.** Merged image from the panels in A. with an overlay of the colour-coded arrows indicating SCFA responders. Scale bars: 50 µm. **D.** Bar plot showing the mean fraction of responding neurons from the total amount of cells in a ganglion that are

immunoreactive for calretinin, nNOS, or neither of these markers (other) (n = 4 ganglia examined). Data are presented as mean ± SEM.

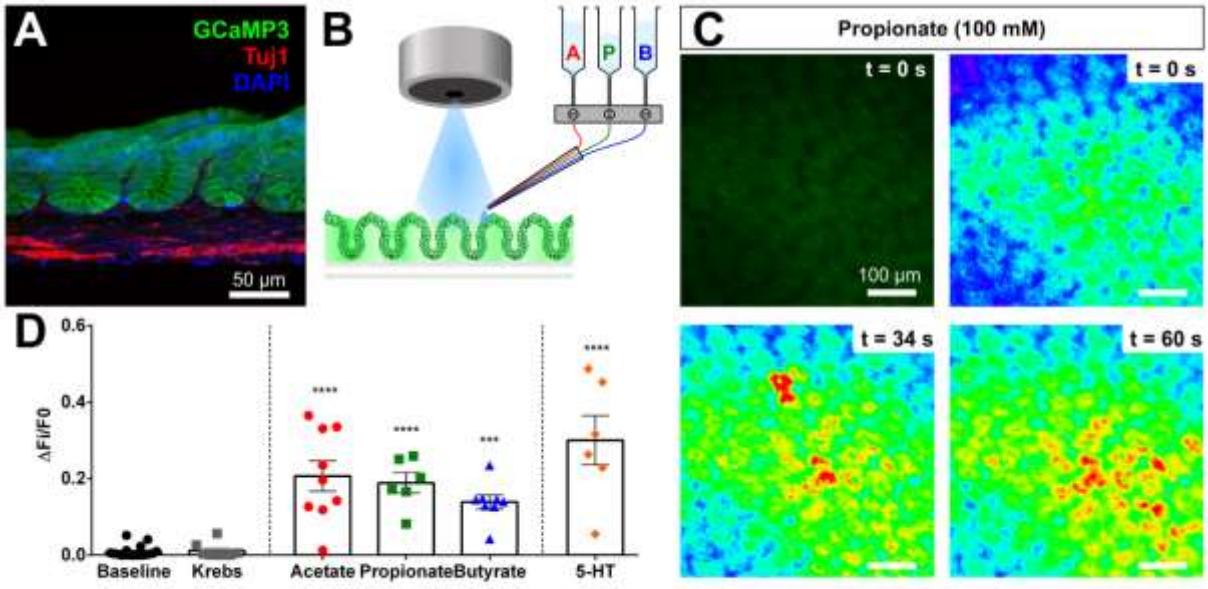

Figure 1.

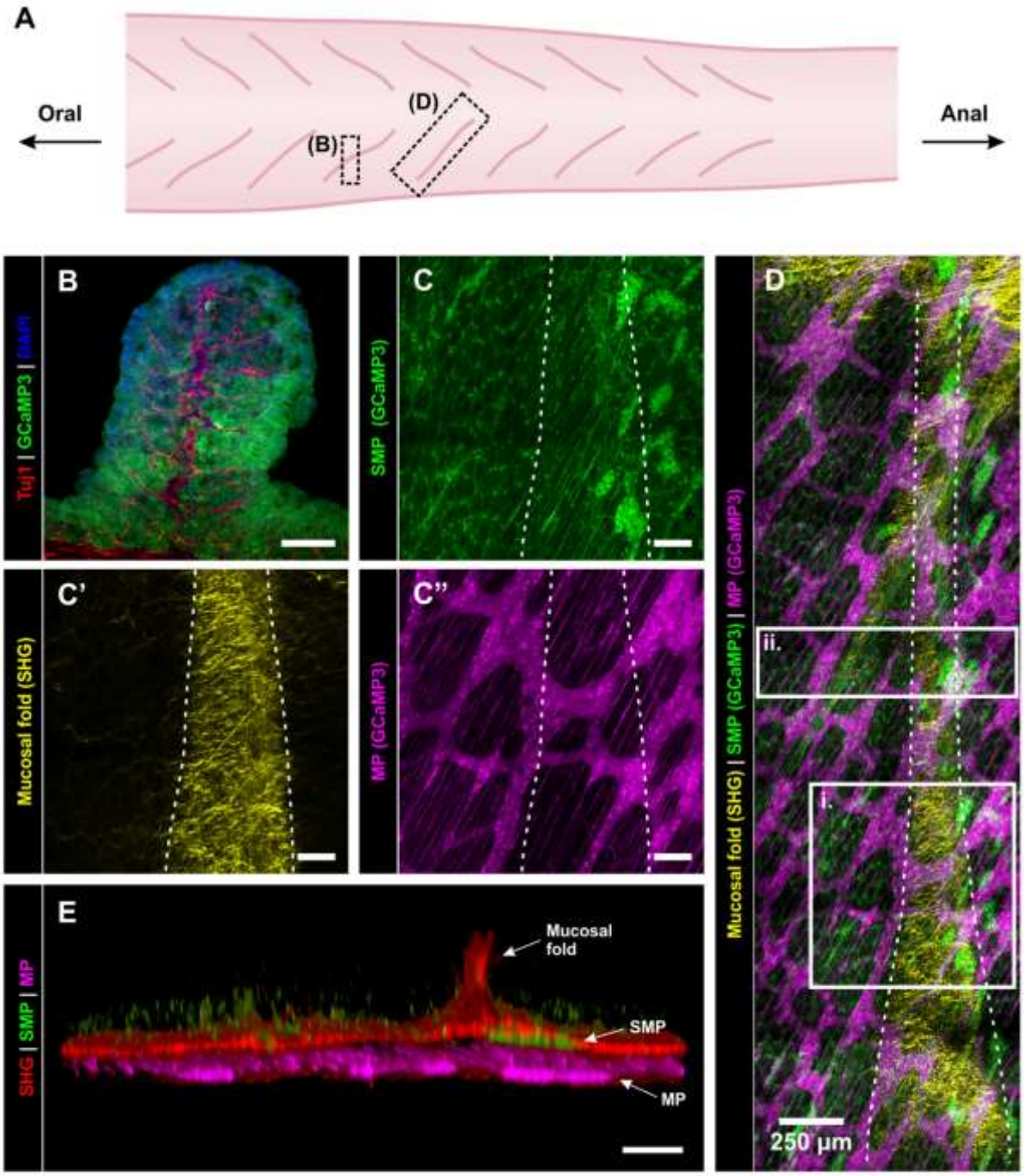
A
Oral
Anal
(B)
(D)
B
TuJ1 | GCaMP3 | DAPI
C
SMP (GCaMP3)
C'
Mucosal fold (SHG)
C''
MP (GCaMP3)
D
Mucosal fold (SHG) | SMP (GCaMP3) | MP (GCaMP3)
ii.
i.
250 µm
E
SHG | SMP | MP
Mucosal fold
SMP
MP

Figure 2.

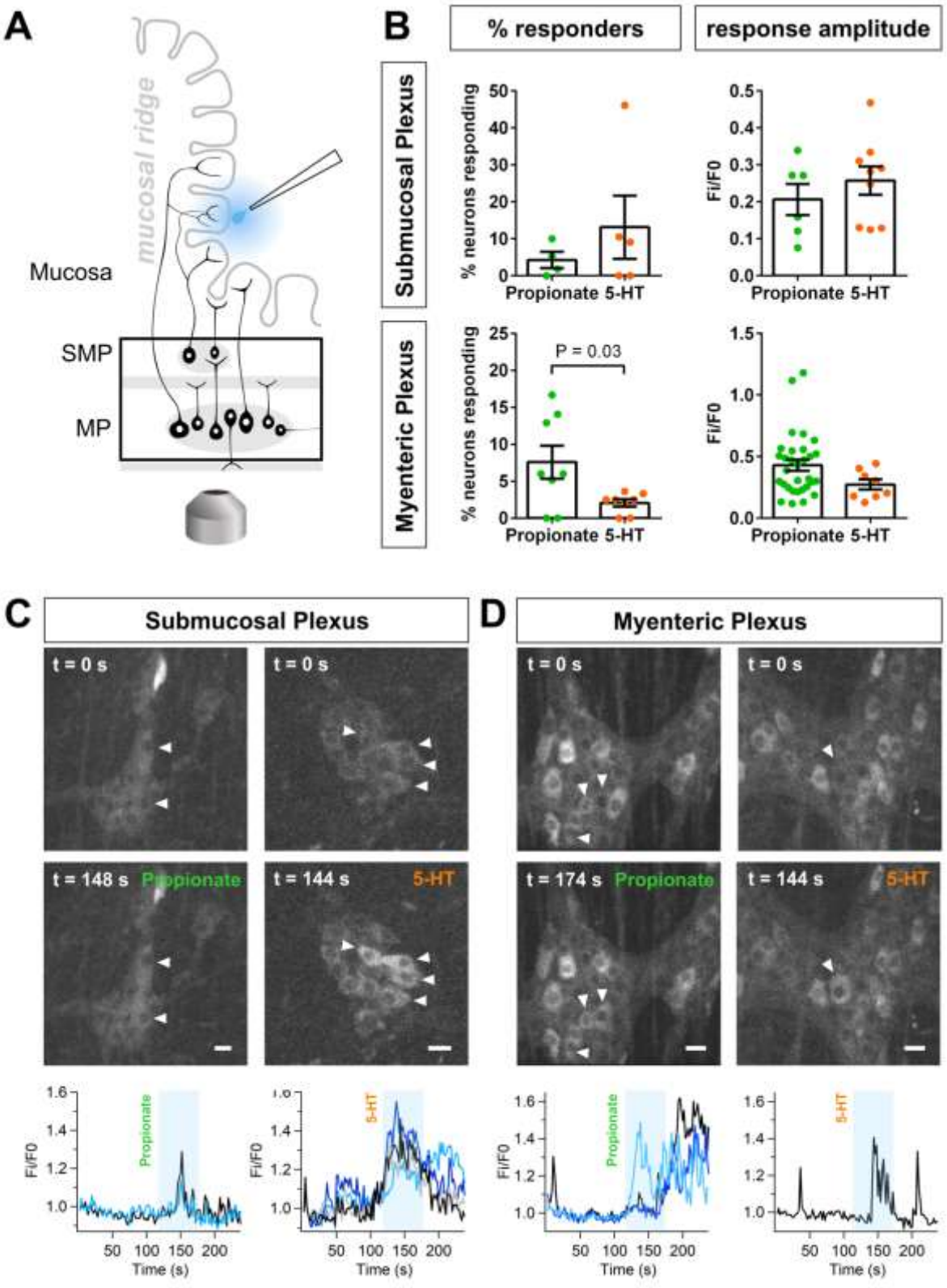
A
mucosal ridge
Mucosa
SMP
MP
B
% responders
response amplitude
Submucosal Plexus
Myenteric Plexus
% neurons responding
Fi/F0
Propionate 5-HT
P = 0.03
C
Submucosal Plexus
D
Myenteric Plexus
t = 0 s
t = 148 s Propionate
t = 144 s 5-HT
t = 174 s Propionate
Propionate
5-HT
Time (s)

Figure 3.

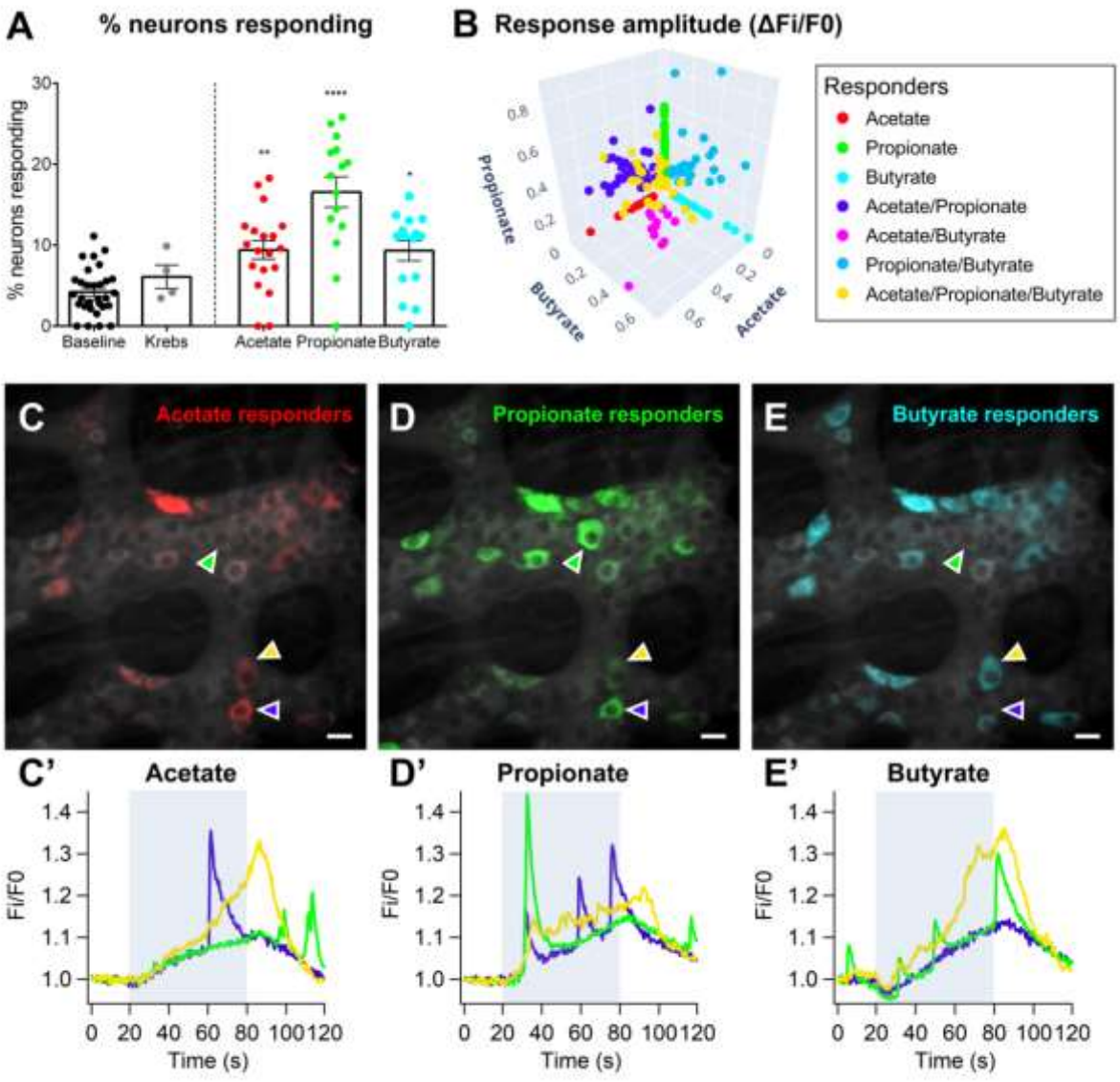
A
% neurons responding
% neurons responding
Baseline
Krebs
Acetate
Propionate
Butyrate
B
Response amplitude (ΔFi/F0)
Propionate
Butyrate
Acetate
Responders
Acetate
Propionate
Butyrate
Acetate/Propionate
Acetate/Butyrate
Propionate/Butyrate
Acetate/Propionate/Butyrate
C
Acetate responders
D
Propionate responders
E
Butyrate responders
C'
Acetate
D'
Propionate
E'
Butyrate
Fi/F0
Time (s)

Figure 4.

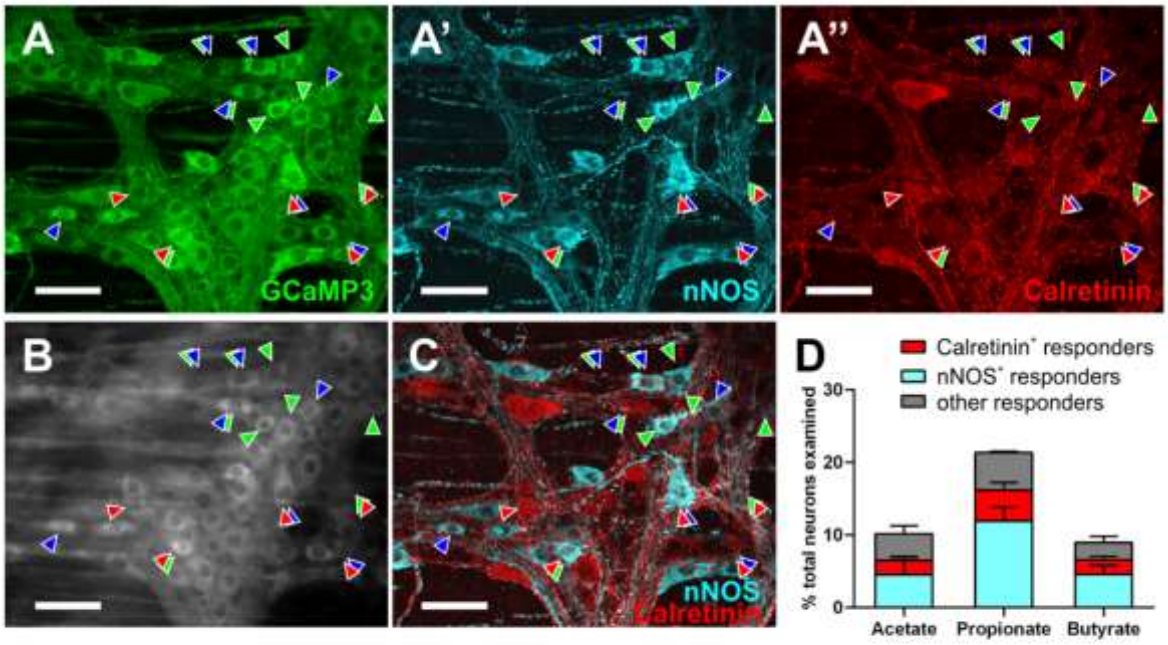
A
GCaMP3
A'
nNOS
A''
Calretinin
B
C
nNOS
Calretinin
D
Calretinin+ responders
nNOS+ responders
other responders
% total neurons examined
30
20
10
0
Acetate
Propionate
Butyrate

Figure 5.